Influence of sediment composition on morphology and internal structure of mixed siliciclastic–bioclastic coastal barriers: Contribution of flume experiments

Alissia Rieux, Pierre Weill, Dominique Mouazé, Bernadette Tessier

SEDIMENTOLOGY the journal of the International Association of Sedimentologists

Sedimentology (2023) **70**, 1580–1600 doi: 10.1111/sed.13083

Influence of sediment composition on morphology and internal structure of mixed siliciclastic–bioclastic coastal barriers: Contribution of flume experiments

ALISSIA RIEUX, PIERRE WEILL, DOMINIQUE MOUAZÉ and BERNADETTE TESSIER
Normandie Univ, UNICAEN, UNIROUEN, CNRS, M2C, 14000, Caen, France (E-mail: alissiarieux@gmail.com)

Associate Editor – Rick Sarg

ABSTRACT

Coastal barriers are dynamic systems, the morphology and architecture of which are controlled by local hydrodynamics, sea-level fluctuations at different timescales, geological heritage and sediment composition. Coastal barriers may be composed of siliciclastic sediments, bioclastic sediments, or a mixture of both. Mixed siliciclastic–bioclastic sediments (as common as 'pure' sediments) are still little represented in the literature. Changes in sediment composition could affect sedimentary processes which are involved in the construction and stability of coastal barriers due to a different hydrodynamic behaviour between bioclastic and siliciclastic particles. In this study, wave-flume experiments were used to investigate the role of sediment compositional mixing on the morphology and architecture of coastal barriers. Three different siliciclastic/bioclastic mixtures were exposed to regular wave forcing, together with mean water level fluctuations to create regressive and transgressive depositional units. Compositional mixtures responded similarly in first-order to mean water-level fluctuations, with the formation of a bar at low water level. Its subsequent on-shore migration and reworking as berm deposits during rising water level stages, and with the formation of washover deposits during high water level stages. In detail, the increasing content of bioclastic sediment increased the beachface slope and reduced the length of washover deposits. The faster aggradation of washover sheets with bioclastic-rich mixtures accelerated the barrier recovery after a submersion and breaching event. A strong segregation between the siliciclastic and the bioclastic grains was observed in the different depositional units, which is attributed both to the coarse size (grain-size control) and to the flat-shape (compositional control) of the bioclastic particles.

Keywords Beach ridge, bioclastic/siliciclastic sand, physical model, stratigraphy, washover.

INTRODUCTION

The increase of ground-penetrating radar studies in the last decades has been a major step forward for the characterization of coastal barrier sedimentary architecture (Jol *et al.*, 1996; Neal, 2004). Ground-penetrating radar provides high-quality subsurface data that helped to constrain depositional models (Weill *et al.*, 2012; Fruergaard *et al.*, 2020) and clastic reservoir heterogeneities (Berton *et al.*, 2019), as well as to reconstruct Holocene sea-level (Tamura, 2012;

Hede *et al.*, 2013; Billy *et al.*, 2015; Costas *et al.*, 2016), storm chronologies (Dougherty, 2014; Goslin & Clemmensen, 2017) and climatic fluctuations (Oliver *et al.*, 2018).

The morphologies and internal structures of coastal barriers reflect the diversity of coastal settings and processes occurring around the world, and their complex interactions at different timescales (Tamura, 2012; Cooper *et al.*, 2018). Wave and wind climate, extreme events, relative sea-level fluctuations, bedrock control, as well as sediment supply are found to be the major controlling factors. However, most of the studies on modern coastal barriers are limited to siliciclastic systems. Modern carbonate coastal barriers are scarce compared with their siliciclastic counterparts (Stutz & Pilkey, 2001). Except for rare barrier islands on carbonate ramps (Rivers *et al.*, 2020), most of the carbonate barriers occur in low wave-energy, tidal environments (open coasts, estuaries or embayments), in the form of bioclastic chenier ridges (Neal *et al.*, 2002; Weill *et al.*, 2012) or bioclastic beach ridges (Jahnert *et al.*, 2012). Mixed siliciclastic–carbonate coastal barriers have received no particular attention, although they are probably frequent features along mixed shelf environments (Larsonneur *et al.*, 1982; Bastos *et al.*, 2015; do Nascimento Silva & Gomes,2020).

Several experimental studies have highlighted the singular behaviour of bioclastic particles, which feature lower settling velocities and lower to a similar threshold of motion compared to siliciclastic particles (Maiklem, 1968; Braithwaite, 1973; Kench & McLean, 1996; Paphitis *et al.*, 2002; Smith & Cheung, 2004; Weill *et al.*, 2010; Joshi *et al.*, 2017; Rieux *et al.*, 2019; Fick *et al.*, 2020; Li *et al.*, 2020; de Kruijf *et al.*, 2021). In mixed depositional systems, these differences lead to sediment partitioning (Flemming, 2017), as recorded for example in the heterolithic stratification of fossil subaqueous dune deposits (Longhitano, 2011; Chiarella & Longhitano, 2012). It is thus reasonable to question whether the composition of mixed siliciclastic–bioclastic sediment is a controlling factor of the sedimentary architecture of wave-built coastal deposits.

This contribution documents a set of flume experiments designed to investigate the effect of sediment composition on the morphology and internal architecture of wave-built ridges. Three different mixtures of bioclastic and siliciclastic material were used, where the bioclastic fraction represented 25%, 50% and 100% of the total sediment composition. For each experiment, the same conditions of regular waves and mean water level fluctuations were applied. Based on elevation profiles and side-view photographs, the morphological responses of the ridges to hydro-sedimentary processes are reported. The preserved deposits are described in terms of compositional and stratal mixing (*sensu* Chiarella *et al.*, 2017) thanks to grain-size analysis, lacquer-peels and side-view photographs. The differences of ridge morphology, internal structures and resilience to changing water level are discussed in relation to the degree of mixing.

MATERIALS AND METHODS

The physical models designed for this study are not properly engineering reduced scale models based on similitude criteria (Hughes, 1993), but rather stratigraphic models based on the principle of similarity (Paola *et al.*, 2009) or relaxed classical scale rules (Kleinhans *et al.*, 2014). Not considering the prolific topic of sediment bedforms, most of the physical experiments on coastal sedimentary systems reported in the literature focus on beach morphodynamics (e.g. Grasso *et al.*, 2011; Baldock *et al.*, 2017; Wang *et al.*, 2020) including groundwater interaction and overwash processes (e.g. Williams *et al.*, 2012; Masselink *et al.*, 2016; Matias *et al.*, 2016), or morphodynamics of tide-dominated environments (Kleinhans *et al.*,2015). However, experiments investigating the fine-scale architecture of wave-built coastal bodies are scarce (Weill *et al.*, 2013; Fick *et al.*, 2021). The aim of the present experiments is to understand the links between sediment composition, processes of sediment transport and sorting, and preserved internal architecture of mixed siliciclastic and bioclastic beach ridges.

Sediment choice and composition

The present study focuses on bioclastic sands from temperate-water to cool-water carbonate environments typically dominated by heterozoan assemblages (Pedley & Carannante, 2006). Bioclastic sands consisting of coral-dominated, tropical photozoan assemblages are not considered here.

Pilkey *et al.* (1967) investigated the carbonate fraction of beach and dune sands along the south-eastern U.S. Atlantic coast. The carbonate

material, dominated by mollusc debris, constituted between 1% and 40% of the total sediment composition. Those authors reported that the carbonate fraction is usually coarser and more poorly sorted than the siliciclastic part of the sediment. This is caused by the flat shape of bioclastic particles, and the great shape diversity of particles with similar intermediate diameters. A bi-modal distribution of the carbonate fractions was also noticed, and attributed to the fact that abrasion of the calcareous material produces fines with few intermediate sizes. These observations have been reported in many other cases (e.g. Carranza-Edwards, 2001) although the details of grain sizes for the carbonate and non-carbonate fractions are not always provided. It also appears that the percentage and size of the bioclastic fraction of beach sands increase in low wave-energy environments where large seagrass meadows (e.g. Short, 2002) or tidal flats (Neal *et al.*, 2002; Weill *et al.*, 2012) promote an intense carbonate production (De Falco *et al.*, 2017), and where shell breaking is moderate. Accordingly, the sediment used in the experiment was composed of an artificial mixture of coarse bioclastic sand and granule, and finer siliciclastic sand.

The bioclastic material was collected on the southern coast of the Mont-Saint-Michel Bay (Brittany, France) on modern chenier ridges composed of coarse to very coarse-grained shell debris and of fine siliciclastic sand reworked from the tidal flat (Bonnot-Courtois *et al.*, 2004; Weill *et al.*, 2012; Tessier *et al.*, 2019). Bioclastic particles consist mainly of fragments of intertidal mollusc bivalve shells. Their faunal composition, settling velocity and threshold of motion are reported in Weill *et al.* (2010) and Rieux *et al.* (2019). The sediment was sieved between 0.63 mm and 4.0 mm to remove the fine siliciclastic fraction and the coarsest bioclastic particles which would not be mobilized efficiently in the flume. The resulting bioclastic fraction has a wide, asymmetrical (skewness = 1.26) unimodal distribution with a modal diameter of 0.63 to 0.8 mm (Fig. 1). The siliciclastic fraction was prepared using two different quarry sands with modal diameters smaller (0.2–0.25 mm) and equal (0.63–0.8 mm) to the bioclastic fraction, resulting in a bimodal distribution. Siliciclastic sand coarser than the bioclastic fraction was not investigated in this study because this situation is unlikely to occur in nature. Indeed, at similar sieve sizes, bioclastic particles are transported more easily than siliciclastic particles (Paphitis *et al.*, 2002; Weill *et al.*, 2010; Rieux *et al.*, 2019; Fick *et al.*, 2020). Bioclastic particles finer than the siliciclastic fraction would thus be winnowed. Where bioclastic particles like mollusc shells are produced *in-situ* in a sandy environment, they are generally coarser than the siliciclastic particles, even after fragmentation.

Three different mixtures were prepared with varying weight percentages of bioclastic sediment: 25%, 50% and 100% (Fig. 1). In the following, these three mixtures are referred to as $B_{25}S_{75}$, $B_{50}S_{50}$ and B_{100} (with B for Bioclastic; S for Siliciclastic). Bulk porosity values of the three mixtures, measured in a 2-l graduated tube, are 29% (±2), 33% (±2) and 44% (±2) for $B_{25}S_{75}$, $B_{50}S_{50}$ and B_{100}, respectively.

Flume setup

Coarse-grained bioclastic coastal barriers generally develop along the coasts of tidal embayments (Neal *et al.*, 2002; Jahnert *et al.*, 2012; Weill *et al.*, 2012), where waves are attenuated by wide intertidal flats (Kirby, 2000; Cooper, 2005; Houser & Hill, 2010), resulting in a quite narrow range of wave heights on the barrier (e.g. Mury *et al.*, 2019). Moreover, such barriers are subject to water level variations, sometimes resulting in tidal flooding and 'non-storm' overwash events (Morton *et al.*, 2000; Weill *et al.*, 2013, 2012; VanDusen *et al.*, 2016). The experiments, performed in an 18 m-long, 50 cm-wide and 65 cm-high glass-sided wave flume (Fig. 2A), were thus designed to reproduce these environmental conditions, by exposing the three compositional mixtures to moderate wave action and low-frequency water level fluctuations.

Wave parameters have been measured by Weill *et al.* (2013) on the sampling site of the bioclastic sediment used in the present experiments (Mont-Saint-Michel bay, north-west France). Significant wave height associated with a cold front residual swell ranged between 30 cm and 40 cm, with peak periods of 4 s and 12 s. The measurements of Mury *et al.* (2019) on the same site during a winter depression reported significant wave heights between 40 cm and 80 cm, with mean zero upcrossing periods between 6 s and 9 s. A Froude scaling of 1:10 was applied to these data, and the results were adjusted with the wave generator capacities and to obtain a satisfying wave breaking. Constant waves were created using a piston wave generator (Fig. 2B) with a period of 2 s and a wave

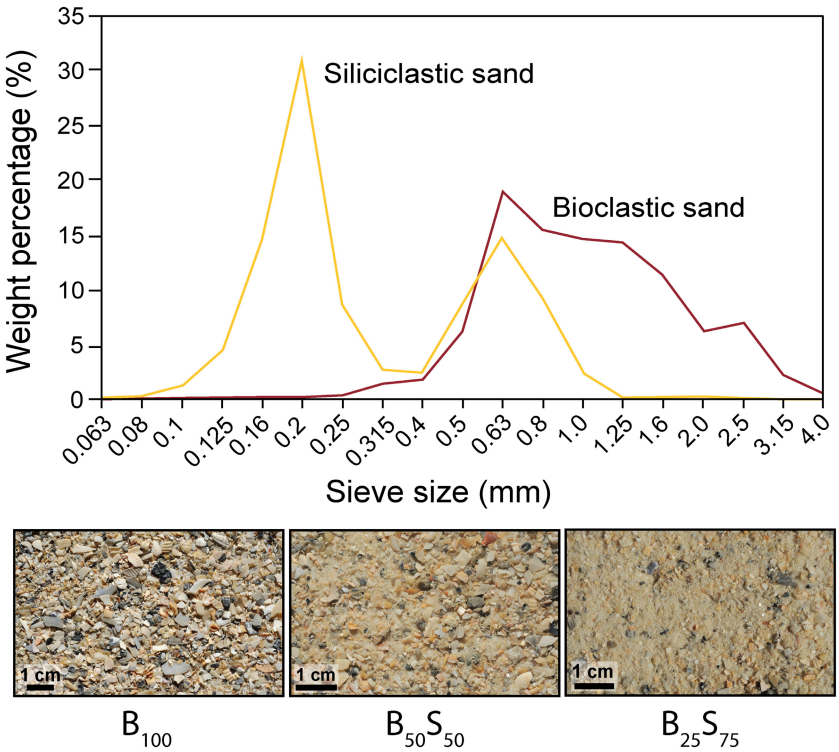

Fig. 1. Grain-size distributions of the bioclastic and the siliciclastic sands used for preparing the three sediment mixtures. Bottom: Photographs of the three sediment mixtures.

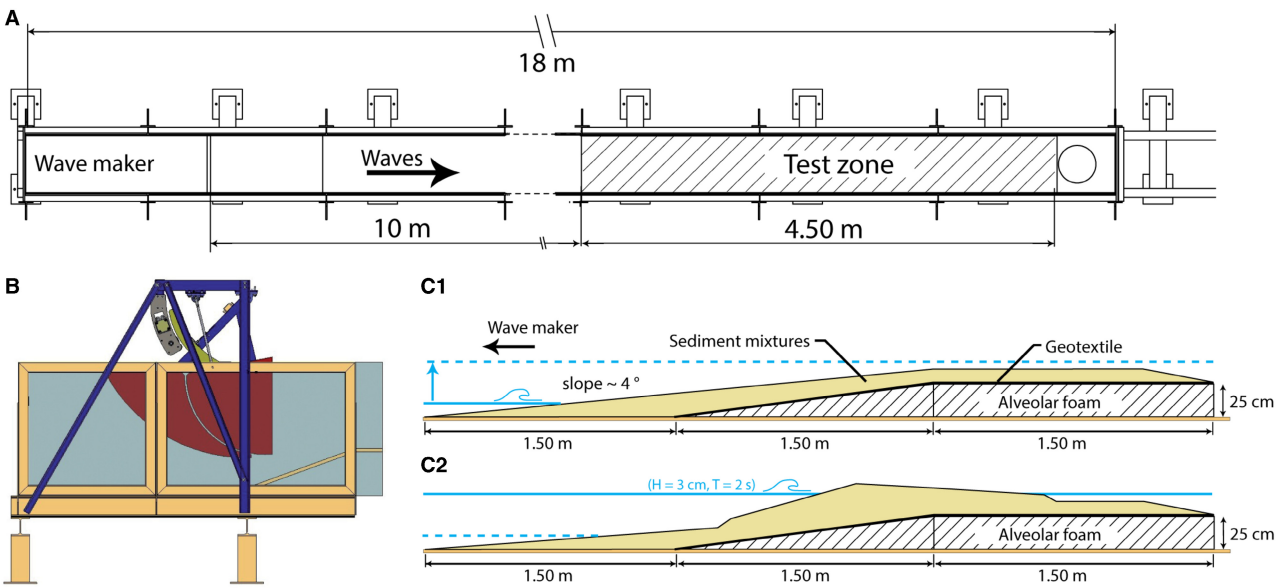

Fig. 2. Experimental setup modified from Weill *et al.*, 2013. Plan view of the wave flume, showing the position of the wave maker and the test zone (A). Side view of the piston wave maker (B). Scheme of the test zone showing the initial beach slope before the experiments (C1) and the wave-built morphology at the equilibrium after raised water level (C2).

height of 3 cm. The wave generator is equipped with an active system which absorbs the major part of the high-frequency reflected waves, and prevents the development of parasite long-standing waves. It also ensures that the generated wave height and period are not affected by

variations of the mean water level. Transformation of wave parameters only occurs in the shoaling zone, depending on the beach profile and reflection coefficient.

To investigate the different modes of barrier construction (progradation versus retrogradation) and the resulting stratigraphy (regressive versus transgressive), cycles of increasing and decreasing water depth (Fig. 3) were simulated by slowly filling or emptying the flume, between 17 cm and 30 cm of water depth. These fluctuations, that are not scaled to any natural cycle of sea-level change, aim at disturbing the equilibrium beach morphology and creating different conditions of sediment deposition, by simulating periods of increased tidal flooding or overwash activity. This approach aims to disturb the equilibrium beach morphology and create different conditions of sediment deposition, by simulating periods of increased tidal flooding or overwash activity. The rate of water level elevation (approximatively 2 mm/min) was chosen to generate overwash events and to allow a progressive adaptation of the barrier, within a reasonable experiment duration. The water level was lowered at the same rate. The duration of water level stability was adjusted to the time required to reach an equilibrium morphology. Consequently, the total duration of the experiment may vary between the different

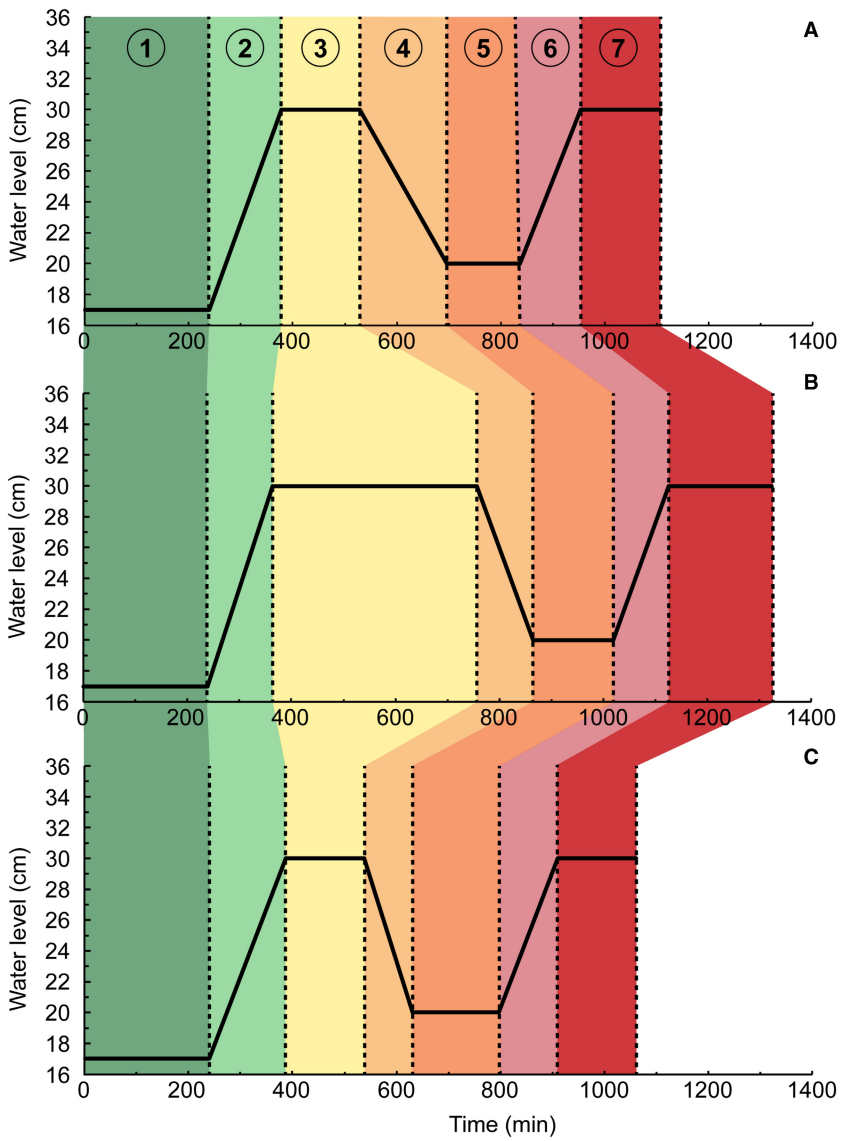

Fig. 3. Mean water level fluctuations in the flume during the three experiments: B_{100} (A); $B_{50}S_{50}$ (B); and $B_{25}S_{75}$ (C). Numbers refer to stages of water level change or stillstand.

compositional mixtures. Hereinafter, a period of variation or stability of the water level is referred as a 'stage'. Stages are numbered similarly in the three experiments, and are reported in Fig. 3.

For each compositional mixing ($B_{25}S_{75}$, $B_{50}S_{50}$ and B_{100}), the sediment was placed on an alveolar foam substrate covered with geotextile (Fig. 2C1) following a slope of 4 degrees. A preconditioning phase (200 min), consisting of slowly filling the flume, with waves, up to 17 cm of water depth, was applied to create a wave-built morphology, defined as the initial state of the experiment (Fig. 2C2).

Morphology and architecture monitoring

At the end of each stage of water level stillstand (Fig. 3 – Stages 1, 3, 5 and 7), the beach ridge morphology was monitored using a laser distance meter (SICK-DT500, Waldkirch, Germany), the distance measurement uncertainty of which is 3 mm. The distance meter was moved manually on a rail along the flume, and was positioned thanks to a code-bar reader with an accuracy of 1 mm. The sampling frequency of the distance meter was 4 Hz, imposing a slow and steady displacement in order to ensure a good density and distribution of the measurement points. The measurements were repeated twice (back and forth) to increase the point density. Five longitudinal profiles, spaced by 9 cm, were measured across the flume (7, 16, 25, 34 and 43 cm) to assess the lateral variability of the morphologies.

Photographs of the glass side walls of the flume were taken regularly (every 10 min on average) to observe the evolution of the internal architecture of beach ridges. In addition, at the end of each experiment, lacquer-peels were made along longitudinal trenches dug in the centre of the flume. The preserved cross-sections are available in Fig. S1. Finally, surface sediment samples (1 cm thick, 200–300 g) were taken at the end of each experiment for grain-size analysis.

RESULTS

This section firstly defines the terminology used hereinafter to designate the main morphological parts of the experimental beach ridges, regardless of the sediment composition (Fig. 4). For more convenience, the term 'seaward' refers to the direction towards the wave maker, and 'landward' to the opposite direction. The modelled beach ridges are composed of: (i) a seaward ridge face including a ridge toe, which corresponds to the breaker zone, and a beachface where the swash and backwash currents occur; and (ii) a landward ridge face composed of washover deposits. An upper washover face, where sediment is essentially by-passing, and a lower washover face where sediment is deposited were differentiated. A shallow lagoon develops landward of the barrier when the water level exceeds 26 cm. The equilibrium morphology was defined as a state where the topography of the ridge does not change with time. Sediment transport occurs on the beachface under the action of wave breaking and swash currents, but the profile is stable. The ridge crest is well-developed and prevents any wave overwashing. The landward ridge face is thus inactive. Interpreted side photographs are used to describe the morphological and internal structure evolutions (Figs 6, 8, 9 and 10); the uninterpreted photographs are available in Figs S4–S7.

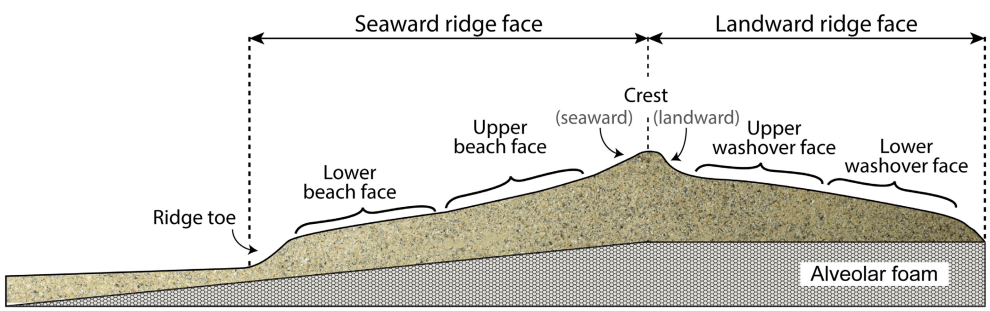

Fig. 4. Morpho-sedimentary elements of the experimental beach ridges.

Morphological evolution and internal architecture

Stage 1 (lowest water level – 17 cm)

Stage 1 corresponds to the reworking of the initial sediment slope (4°) after 240 min of wave exposition at a low water level (17 cm, Fig. 3). Sediment is eroded at the wave breaking point, and deposited on the upper swash zone where particle segregation occurs: coarse-grained bioclastic particles are deposited on the most distal part of the swash zone, whereas finer-grained and/or siliciclastic particles remain mobile in the lower beach profile. With B_{100}, the rapid accumulation of coarse-grained bioclastic particles results in the deposition of aggrading and prograding seaward-dipping beds which constitute a steep (*ca* 13°, Fig. 5) and short (*ca* 60 cm; Fig. 6A) beachface. With $B_{50}S_{50}$ and $B_{25}S_{75}$, the ridge thickens along with the deposition of transgressive, slightly seaward dipping to slightly landward dipping beds (Fig. 6B and C) coarsening landward with a greater bioclastic content. The landward terminations of the transgressive beds are downlapping the initial 4° surface for $B_{50}S_{50}$, while they are onlapping the initial surface for $B_{25}S_{75}$. The seaward terminations are erosional for $B_{50}S_{50}$ and $B_{25}S_{75}$ due to the retrogradation of the beachface. The upper beach profile is constructional for $B_{50}S_{50}$ (aggrading to prograding deposits), while it remains purely erosional for $B_{25}S_{75}$. The stabilization of $B_{50}S_{50}$ and $B_{25}S_{75}$ ridges comes with a thin (*ca* 1 cm) conformal deposit on the beachface. The length and the slope value of the beachface are 85 cm and 12° for $B_{50}S_{50}$, and 88 cm and 9° for $B_{25}S_{75}$ (Fig. 5). While the crest elevations are similar for the three compositional mixtures, their positions are shifted landward with increasing siliciclastic content (Fig. 7), as revealed by the transgressive nature of $B_{50}S_{50}$ and $B_{25}S_{75}$ deposits (Fig. 6B and C).

Stage 3 (high water level – 30 cm)

Stage 3 is a high water level following a *ca* 135 min water level rise between 17 cm and 30 cm of water depth. The duration of Stage 3 is different for each compositional mixing (240, 392 and 150 min for B_{100}, $B_{50}S_{50}$ and $B_{25}S_{75}$, respectively; Fig. 3), because it is related to the time required to reach an equilibrium morphology. For the three compositional mixings, the water level rise resulted in frequent overwashing of the ridge crest, erosion of the beach face and washover fan deposition. The ridges experienced a landward migration by rollover, with a complete reworking of Stage 1 barriers (Figs 6 and 7).

Mixture B_{100} reached an equilibrium morphology at 528 min, i.e. 150 min after the water level stabilized (Fig. 3A), with a barrier width of 125 cm and a beach face slope of 13°. $B_{50}S_{50}$ reached equilibrium at 745 min (380 min after water level stabilization) with a barrier width of 165 cm and a beach face slope of 12.5°. For $B_{25}S_{75}$, Stage 3 was stopped at 537 min before reaching equilibrium because the ridge landward face approached the extremity of the flume test section (alveolar foam, Fig. 2). The barrier width was 170 cm and the beach face slope was 13°.

Disregarding the sediment composition, and compared to Stage 1, the width of the beach ridges increased by elongation of their landward faces related to the deposition of washover fans (Figs 5 and 8).

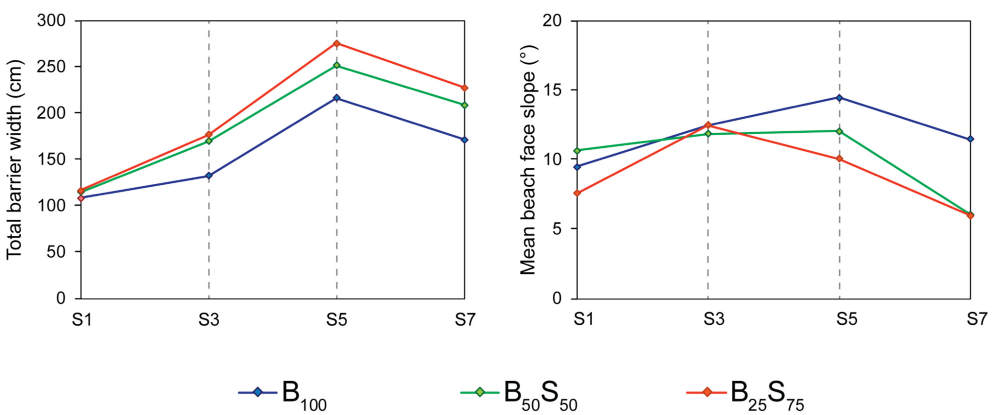

Fig. 5. Evolution of barrier total width and beachface slope values through water level stages for the three experiments.

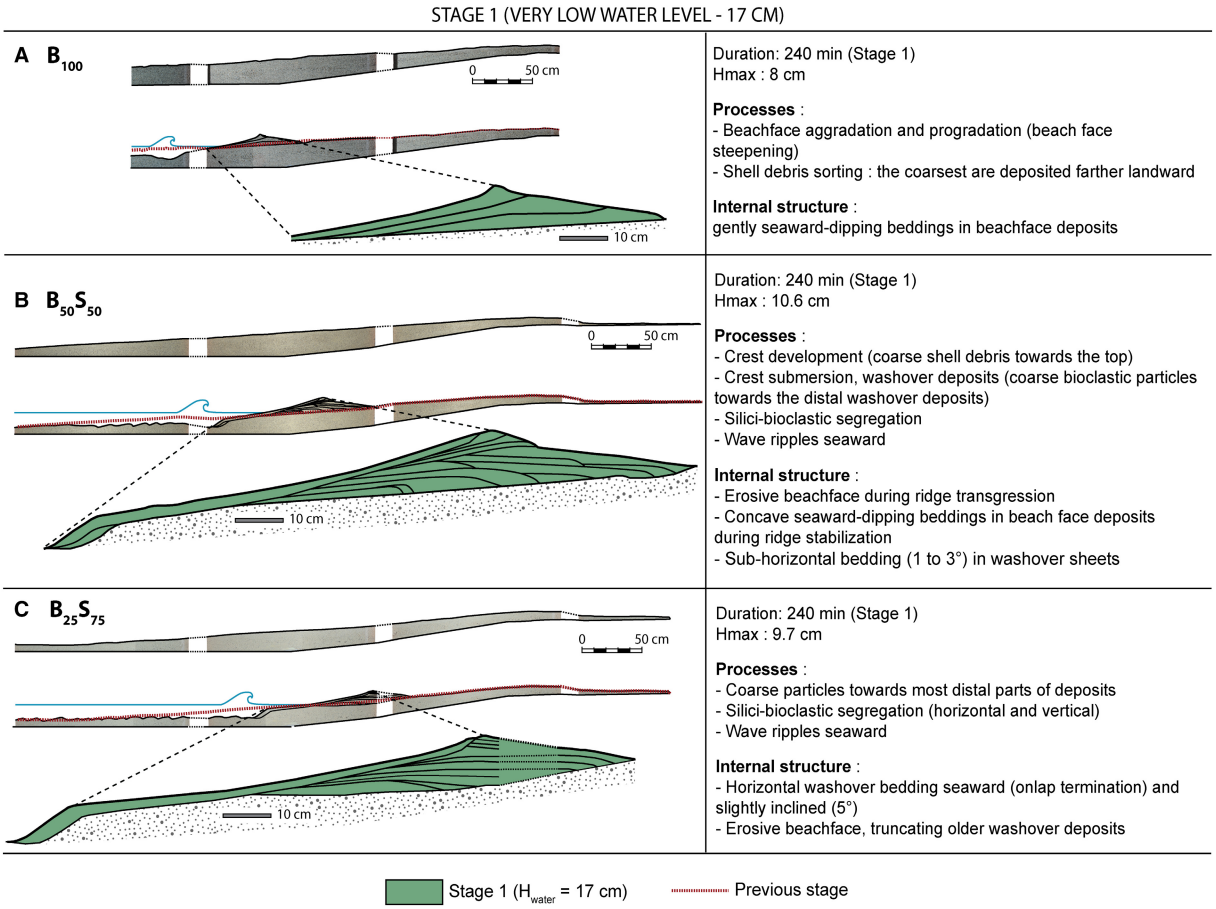

Fig. 6. Internal architecture of the B_{100} (A), $B_{50}S_{50}$ (B) and $B_{25}S_{75}$ (C) barriers at the end of Stage 1.

Ridges at the end of Stage 3 mainly consist of washover deposits and their architectures show some significant differences between the three compositional mixings. B_{100} features thick (one to several centimetres) sub-horizontal to slightly landward-dipping (1–4°) washover sheets, contemporary of Stage 2 water level rise, truncated seaward by the erosive beach face (Fig. 8A). The washover deposits are coarsening-landward, and are strongly aggrading. The length of the deposits decreases upward, resulting in the backstepping of the washover sheets up the landward slope of the ridge, and a subsequent coarsening-upward sequence. Some beachface deposits are preserved during Stage 3. $B_{50}S_{50}$ ridge shows *ca* 1 cm thick series of gently-landward-dipping washover sheets, ending in their most distal part in thicker high-angle foreset beds (Fig. 8B). Individual washover deposits are coarsening landward, together with a greater bioclastic content. The washover deposits are aggrading, but also prograding landward. Consequently, the distal washover foresets are progressively topped by more proximal, finer and siliciclastic washover sheets. Washover deposits occurred mainly during Stage 2, and Stage 3 deposits are a transition between washover sheets, berm and beachface deposits accompanying the recovery of the ridge crest (Fig. 8B).

Washover sheets in $B_{25}S_{75}$ ridge are thin (<1 cm thick), fine-grained and siliciclastic. Coarse bioclastic particles accumulate in the most distal part of the washover as high-angle foreset beds. Preserved washover deposits are associated with Stage 3, the former Stage 2 deposits being reworked by erosive overwash flows (Fig. 8C). The beachface is purely erosional, and the ridge is still retreating landward at the end of Stage 3.

Stage 5 (low water level – 20 cm)

Stage 5 is a *ca* 150 min low water level following a water level drop between 30 cm and 20 cm (Fig. 3). For the three compositional

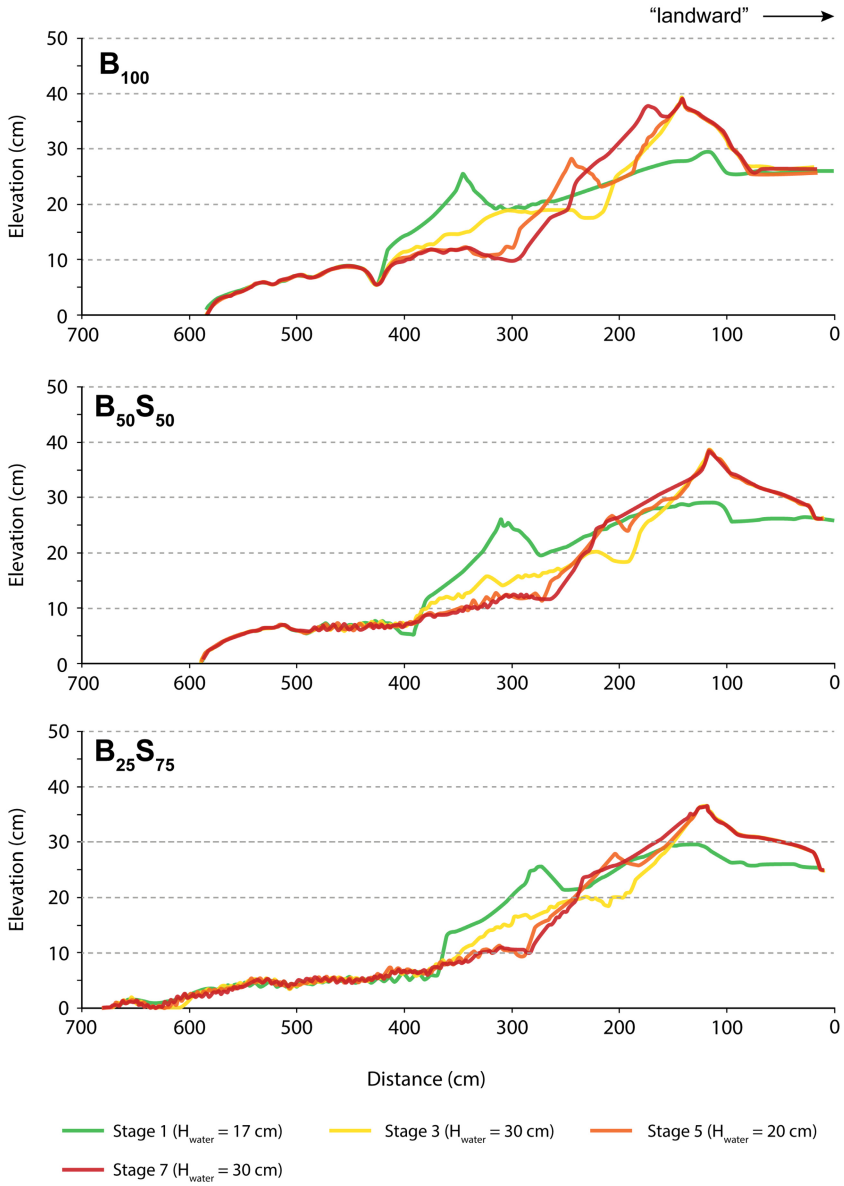

Fig. 7. Longitudinal topographic profiles at the centre of the flume: B_{100}, $B_{50}S_{50}$ and $B_{25}S_{75}$.

mixings, the water level drop (Stage 4) resulted in the abandonment of the former highstand ridge, and the subsequent development of lowstand wave-built sediment accumulation (Stage 5). The whole barriers at the end of Stage 5 are thus composed of a highstand beach ridge and a lowstand beach ridge, more or less connected by a thin falling-stage unit (Fig. 9). The width of the lowstand ridges increases with increasing siliciclastic content in the compositional mixing (63 cm, 81 cm and 93 cm for B_{100}, $B_{50}S_{50}$ and $B_{25}S_{75}$, respectively, Fig. 5). The slope angle of the lowstand beach-face decreases with increasing siliciclastic content (13.5, 10.7 and 10.5° for B_{100}, $B_{50}S_{50}$ and $B_{25}S_{75}$, respectively, Fig. 5).

The falling-stage (Stage 4) deposits of B_{100} are limited to a thin regressive veneer of coarse bioclastic particles on top of Stage 3 beachface (Fig. 9A-1). Subsequently, during Stage 5, the erosive toe of the highstand ridge is filled by aggrading deposits (Fig. 9A-2), which allow the development of the low-water ridge by the progressive steepening of beachface deposits (Fig. 9A-4). Stage 4 deposits are better preserved for $B_{50}S_{50}$ and $B_{25}S_{75}$. They consist of a set of thin and elongated regressive beds (Fig. 9B-1 and 9C-1) of coarse-grained bioclastic particles, downlapping the former fine-grained siliciclastic highstand beach face, as well as the former coarse-grained ridge toe (Figs 9B-2, 9C-2, S2 and S3).

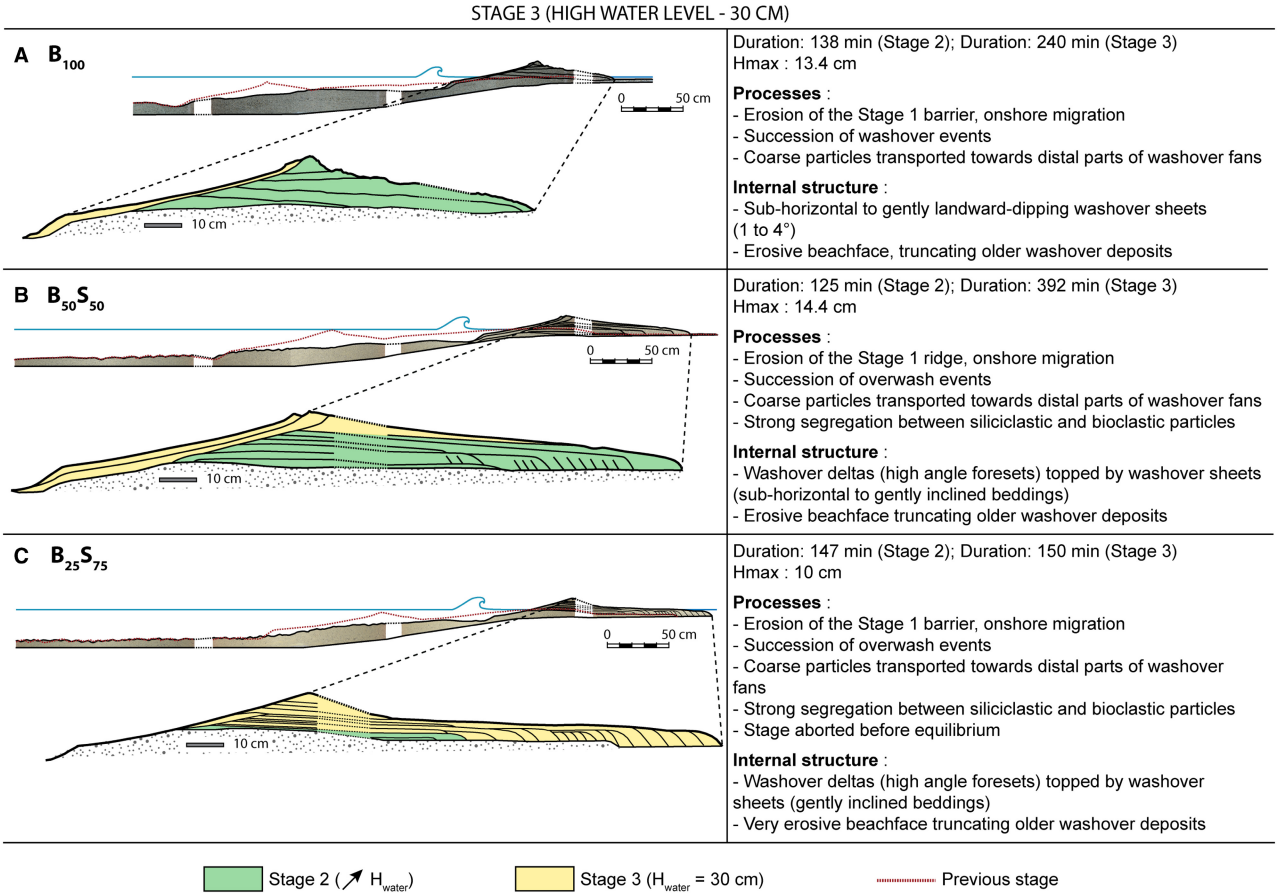

Fig. 8. Internal architecture of the B_{100} (A), $B_{50}S_{50}$ (B) and $B_{25}S_{75}$ (C) barriers at the end of Stage 3.

The lowstand ridges consist of beachface deposits (Fig. 9B-3 and 9C-3) and washover deposits onlapping the regression surface (Fig. 9B-4 and 9C-4).

Stage 7 (high water level – 30 cm)

Stage 7 is a high water level following a *ca* 110 min water level rise from 20 to 30 cm (Stage 6, Fig. 3). The rising water level of Stage 6 resulted in the reworking of Stage 5 lowstand ridges, which migrated landward on top of Stage 3 highstand beachface deposits and Stage 4 regression surface (Fig. 10). Because water level at Stage 7 was not higher than that at Stage 3 (Fig. 3), the former highstand (Stage 3, Fig. 3) barrier crest was not breached or overwashed during the Stage 7 highstand. Consequently, the stacking pattern of the entire barrier at the end of Stage 7 is progradational.

The reworking and retrogradation of the Stage 5 lowstand ridges during Stage 6 led to the formation of washover deposits, the geometries of which differ between the three compositional mixings. B_{100} shows thick (2–3 cm), fining-upward foreset beds downlapping the transgression surface (Fig.10A-1). The foreset beds progressively evolve into gently landward dipping washover sheets (Fig. 10A-2) above the static water level. The new highstand ridge is 92 cm wide, and the beachface slope is *ca* 13° (Fig. 5). The thickness of washover foreset beds decreases with increasing siliciclastic content for $B_{50}S_{50}$ (*ca* 2 cm) and $B_{25}S_{75}$ (*ca* 1.5 cm). Compared to B_{100}, the $B_{50}S_{50}$ and $B_{25}S_{75}$ sediments reworked from the lowstand ridges (Stage 5) are more extensively redistributed upslope along the former beachface of the Stage 3 highstand ridges (Fig. 10B and C). Consequently, no landward face is observed on the Stage 7 ridges of $B_{50}S_{50}$ and $B_{25}S_{75}$. The final length and slope angle of Stage 6/7 deposits are 110 cm, 8° respectively for $B_{50}S_{50}$, and 93 cm, 7° respectively for $B_{25}S_{75}$ (Fig. 5).

Grain-size analysis of the final beach ridges

Surface sediment samples have been collected for grain-size analysis along the final stage beach

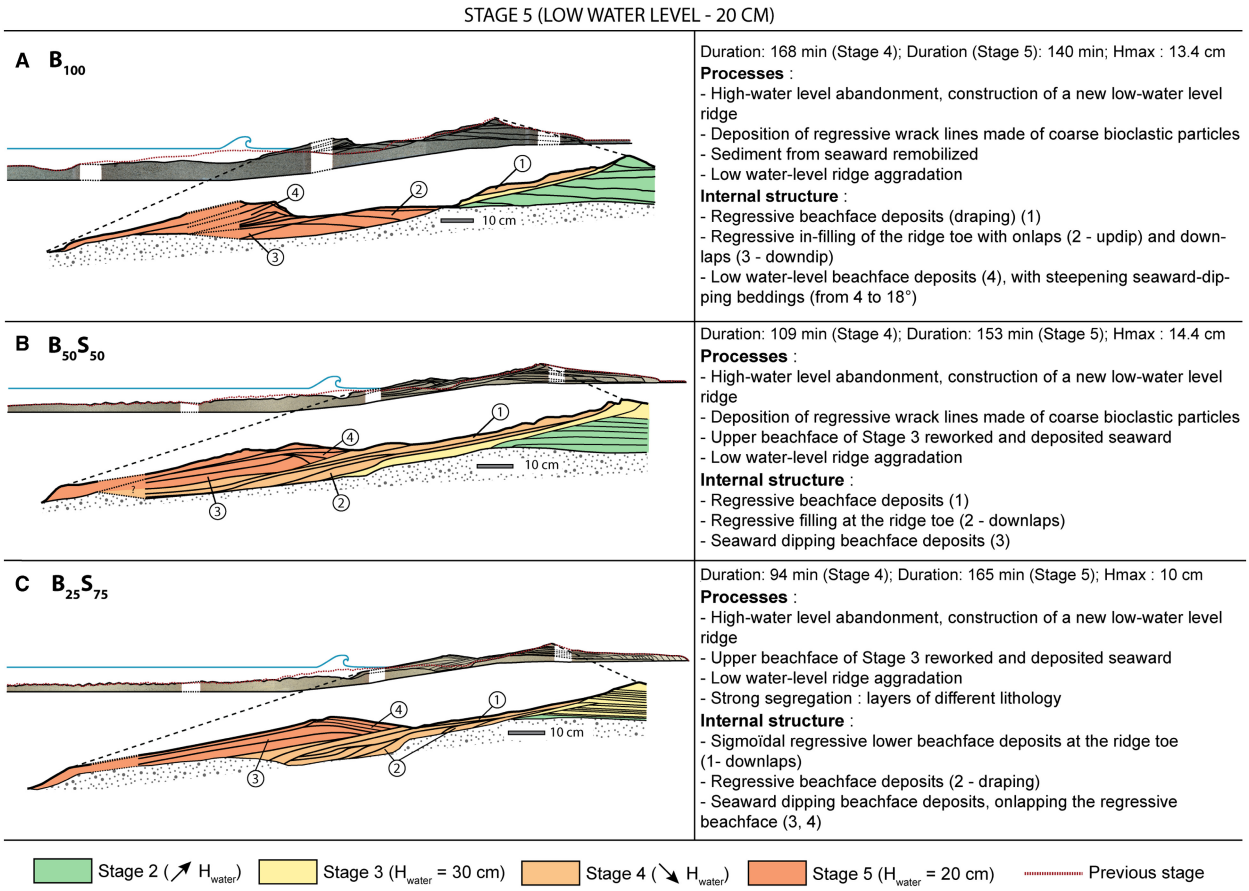

Fig. 9. Internal architecture of the B_{100} (A), $B_{50}S_{50}$ (B) and $B_{25}S_{75}$ (C) barriers at the end of Stage 5.

ridges (Fig. 11 for $B_{50}S_{50}$, Figs S8 and S9 for B_{100} and $B_{25}S_{75}$, respectively). It is important to remember that, for compositional mixtures $B_{50}S_{50}$ and $B_{25}S_{75}$, the coarse fraction (>1.25 mm) is purely bioclastic, while for sediment finer than 0.25 mm it is purely siliciclastic.

The grain-size trends are first described from the $B_{50}S_{50}$ experiments. Seaward of the ridge toe (Fig. 11A), the sediment surface shows an enrichment of fine siliciclastic particles, and of very coarse bioclastic particles (>2.5 mm). The ridge toe and the lower beachface (Fig. 11B and C) are significantly enriched in coarse bioclastic particles. The intermediate beachface (Fig. 11D and E) is better sorted than the initial sediment, and enriched in mixed-composition medium grain-size sand (0.4–1.0 mm). The ridge crest (Fig. 11F), which is not active at the final stage, is poorly sorted and coarser than the initial sediment. Finally, the washover surfaces are very coarse and completely depleted in fine siliciclastic sediment.

With B_{100}, the sorting is less spectacular (Fig. S8), as the initial sediment is by definition mono-compositional and better sorted than $B_{50}S_{50}$. The ridge toe and lower beachface (Fig. S8B and C) are close to the initial sediment grain-size distribution. The upper beachface and active ridge crest (Fig. S8D and E) are significantly enriched in coarse bioclastic particles. The washover face (Fig. S8F and G) is coarsening towards its distal part.

Considering the $B_{25}S_{75}$ compositional mixture, the ridge toe and the lower beachface (Fig. S9B and C) are finer than the initial sediment. However, the coarse body of sediment preserved below suggests that the surficial texture is not representative of the construction stage. On the upper beachface (Fig. S9D), the bimodal distribution of the initial sediment is still visible, although enriched with coarse bioclastic particles. The landward ridge face shows a clear coarsening trend from the ridge crest (Fig. S9E and F) to the washover termination (Fig. S9H) where no siliciclastic sediment is preserved.

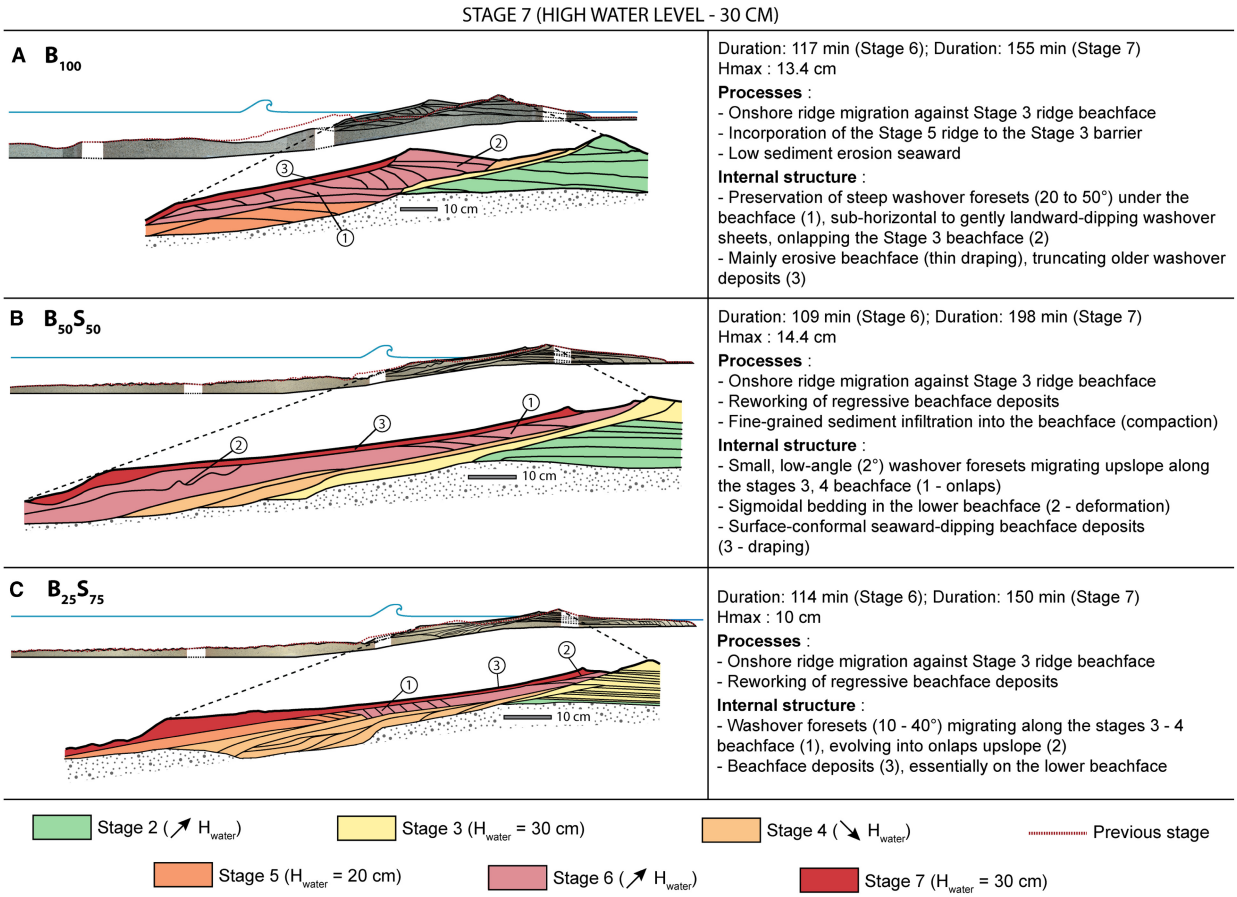

Fig. 10. Internal architecture of the B_{100} (A), $B_{50}S_{50}$ (B) and $B_{25}S_{75}$ (C) barriers at the end of Stage 7.

DISCUSSION

Ridge stratigraphy

The ridge structures obtained for the three compositional mixtures developed similarly in response to mean water level fluctuations. The first stages of water level rise and highstand (Stages 2 and 3, Fig. 12) resulted in the formation of transgressive deposits with gently landward-dipping washover sheets and steeper washover delta foresets. The transition between washover sheets (subaerial deposits) and foresets (submerged deposits) is related to the level of the back-barrier pond or lagoon (Schwartz, 1982; Matias *et al.*, 2014). The washover deposits form a coarsening-upward sequence, as the result of backstepping of individual washover sheets (Fig. 13). This is associated with the progressive reduction of washover flow intensity, due to the healing of the crest breach, and to the increasing infiltration of washover flow as the ridge landward face thickens by aggradation above the static water level. Falling stage (Stage 4, Fig. 12) preserved little deposits except for a coarse lag deposit on the beachface, and regressive deposits associated with the seaward translation of the ridge toe. Lowstand (Stage 5, Fig. 12) resulted in the emergence of a sediment bar or ridge which is largely reworked by subsequent water level rise (Stage 6, Fig. 12) and poorly preserved. The retrogradation and reworking of the lowstand ridge led to the complete or partial covering of the initial highstand beachface.

To the authors' knowledge, the only experimental work that shows some similarities with our study, and the findings of which could be compared with our results, have been published by McKee & Sterrett (1961). Those authors investigated in a wave flume the emergence and structures of longshore bars made of fine-grained quartz sand, and the way they interact with beaches, under varying conditions of water depth, wave energy and sediment supply. They showed

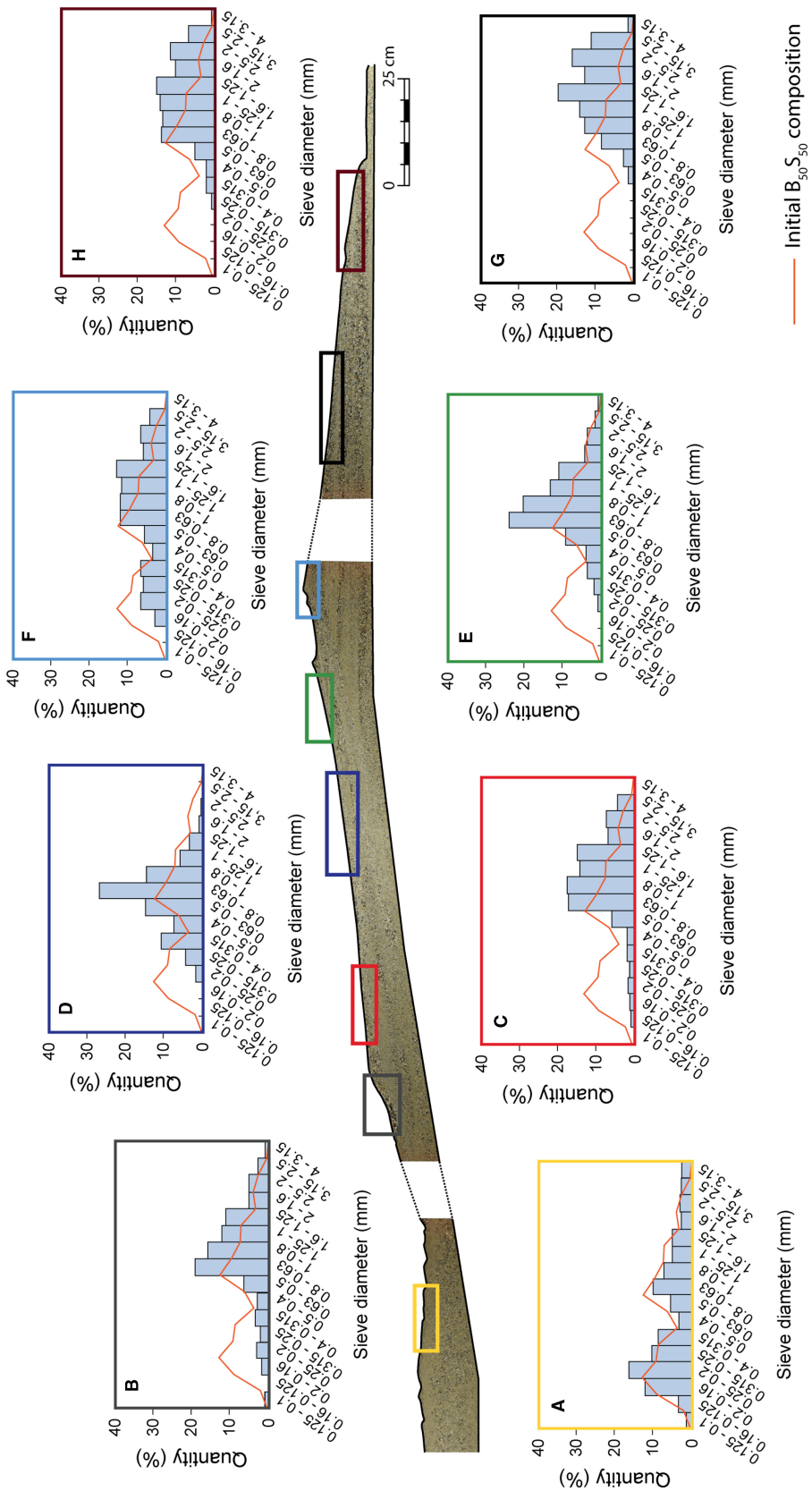

Fig. 11. Grain-size evolution along the final $B_{50}S_{50}$ barrier surface. The same grain-size distribution is obtained for the three experiments. The illistrations for B_{100} and $B_{25}S_{75}$ are provided in Figs S1–S9.

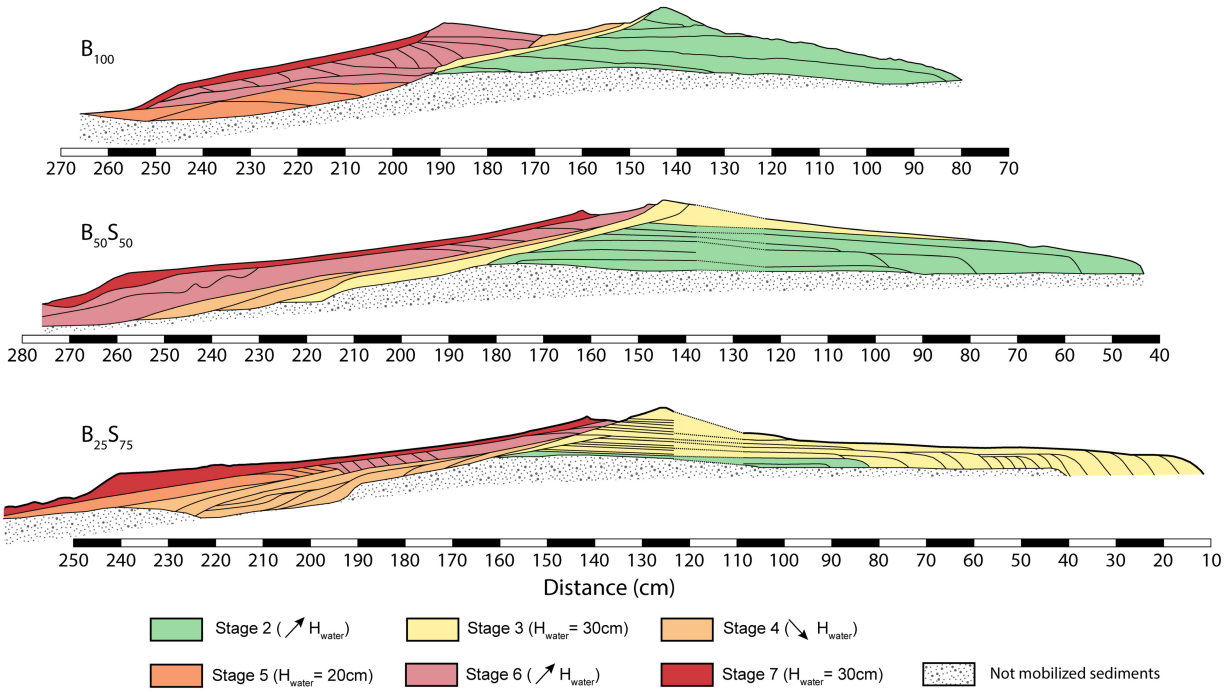

Fig. 12. Interpreted internal architectures of the B_{100}, $B_{50}S_{50}$ and $B_{25}S_{75}$ barriers at the end of Stage 7. The 0 position corresponds to the end of the flume test section, opposite to the piston wave maker.

that under shallow-water conditions, an emergent bar forms around the point of wave break relatively far from shore and migrates landward with the deposition of landward-dipping foreset beds. Under moderate wave energy, the bar stabilizes on the shoreface, isolating a lagoon in front of the beach. With increasing wave energy, the bar migrates onto the beach, and no lagoon forms. With increasing sediment supply under shallow water and moderate wave energy, the bar thickens and the basal foreset beds progressively evolve into gentle seaward-dipping beds. In conditions of deep water, no bar forms and the supplied sand is progressively transported towards the beach, promoting the sedimentation of the beachface, and the development of a wide shoreface terrace composed of prograding foreset beds. The reported structures of emerging bars at shallow depth show numerous similarities with ridges developing during lowstand in the present study (Stage 5, Fig. 9). Their subsequent reworking with increasing water level led to internal structures (Stage 7, Fig. 10) similar to that reported by McKee & Sterrett (1961) under deep water conditions. In the field, beach ridge structures showing significant landward-dipping deposits are generally associated with the development, landward migration and welding of swash bars under fair-weather conditions (Hine, 1979; Carter, 1986; Bristow *et al.*, 2000; Lindhorst *et al.*, 2008; Tamura, 2012; Fruergaard *et al.*, 2020), in coastal settings with significant (>1 m) tidal range (Masselink *et al.*, 2006). The dynamics of swash bars, and consequently the way they contribute to the construction of coastal ridges, are principally controlled by the tidal water levels, as they control the duration of the wave processes operating on the cross-shore profile (Masselink *et al.*, 2006). In a macrotidal environment, this duration exhibits significant long-term fluctuations associated with the 18.6-year nodal tidal cycle, which may influence the decadal behaviour of ridge construction (Weill *et al.*, 2012).

Sediment sorting – Grain-size or compositional control?

In the proposed experiments, the same segregation processes were observed regardless of the compositional mixture or water level stage. Coarse bioclastic particles were deposited on the lower and upper beach face, on the ridge crest and on the distal parts of washover fans.

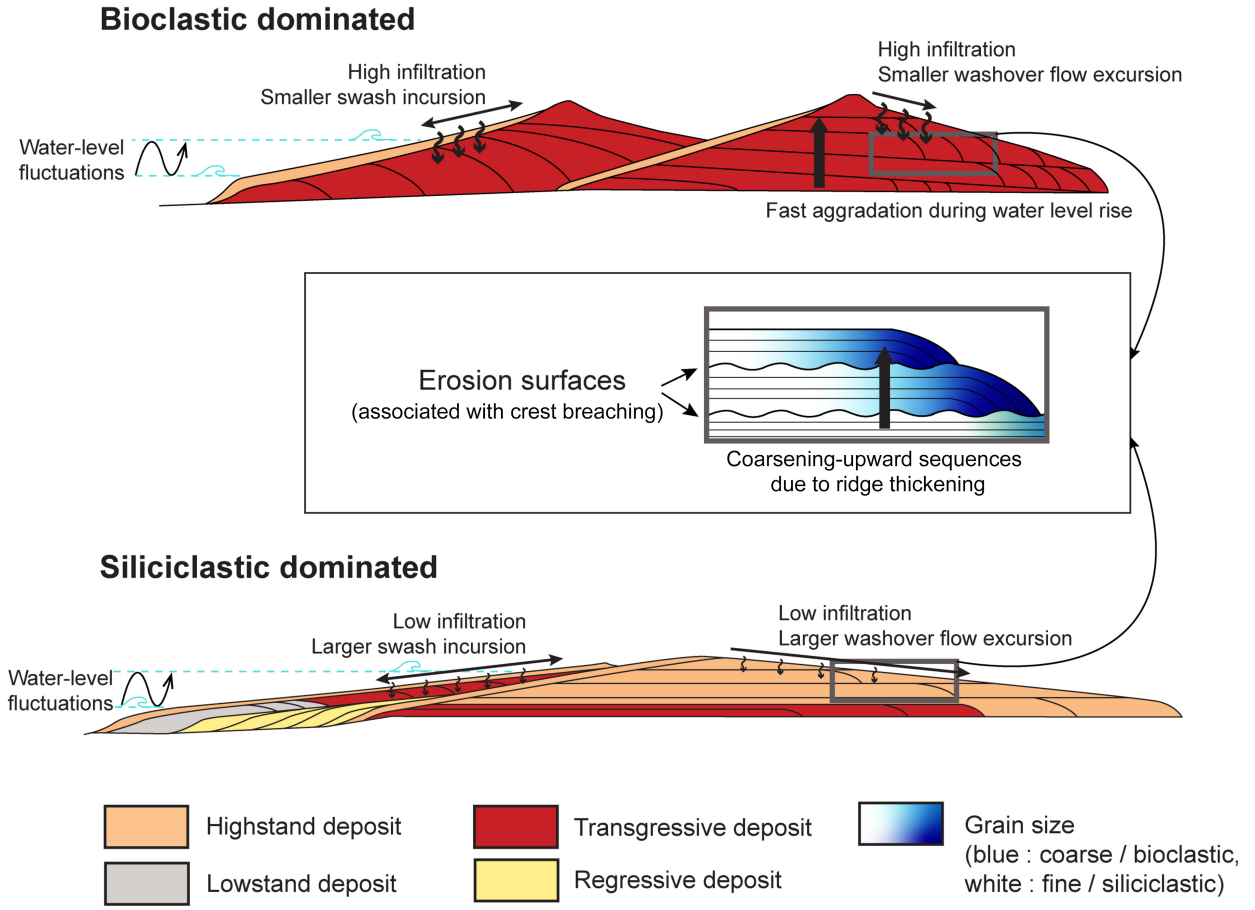

Fig. 13. Synthetic scheme showing morphology and architecture differences between bioclastic and siliciclastic-dominated barriers.

Siliciclastic sands and finer bioclastic particles were generally associated with more energetic areas (swash zone, proximal washover fans), where the coarsest bioclastic particles were bypassing. Given the initial grain-size distribution of the sediment mixtures, where the coarsest fraction is bioclastic and the finer fraction is siliciclastic, it is reasonable to question whether the observed segregation is controlled by the grain-size or by the sediment composition. In other words, would the same sorting trends have occurred in the case of a purely siliciclastic sediment?

Several sorting mechanisms are recognized to occur in the swash zone (Slingerland & Smith, 1986; Komar, 1989): suspension sorting, entrainment sorting, transport sorting and shear sorting. Suspension sorting is related to the settling velocity of particles. Bioclastic particles have lower settling velocities than siliciclastic particles of similar size (e.g. Weill *et al.*, 2010; Rieux *et al.*, 2019; de Kruijf *et al.*, 2021). Coarse platy bioclastic particles of the reported experiments, in the range of *ca* 0.5 to 2.0 mm, are equivalent to sub-rounded siliciclastic particles in the range of *ca* 0.25 to 0.75 mm in terms of settling velocity (Fig. 3 in Weill *et al.*, 2010). Suspension sorting is probably negligible in the experimental swash zone due to the very small thickness of the flow. Moreover, the bioclastic nature of the sediment (through particle shape) tends to reduce the differences of settling velocity between the two grain-size fractions of the compositional mixtures. Transport sorting is somehow equivalent to settling sorting in the horizontal direction, as the grain transport velocity is related to the ratio between the particle submerged weight and its projected surface. Thin and platy bioclastic particles are transported further in the swash zone than

siliciclastic particles of similar sizes would be. Similar interpretations were proposed by Chiarella & Longhitano (2012) to explain the segregation between bioclastic and siliciclastic particles, and subsequent heterolithic stratification observed in fossil tidal dunes. Entrainment sorting is related to the threshold of motion of sediment particles. Numerous studies have shown that shear stress values of bioclastic particles fall below the predictive curves for siliciclastic sediments (Paphitis *et al.*, 2002; Smith & Cheung, 2004; Weill *et al.*, 2010; Rieux *et al.*, 2019). Finally, shear sorting, sometimes referred to as kinetic sieving, corresponds to the vertical segregation of a mobile granular bed sheared by a fluid, resulting in a coarsening-upward sediment layer. Owing to smaller pivoting angles, the largest particles roll more easily on the top of the sediment mixture than finer particles trapped in the bed roughness. To the authors' knowledge, the effect of particle shape on shear sorting has not been studied. However, it is expected that platy bioclastic particles have a smaller 'rollability' than more rounded siliciclastic particles. Overall, the preferential transport of the coarse bioclastic fraction and its deposition in the most distal parts of the swash zone and washover fans is controlled both by the shape (related to the sediment lithology) and the size of sediment particles. The accumulation of coarse bioclastic particles in the breaker zone (beach step) have been reported in numerous studies, as the result of fines being removed in this energetic and turbulent zone (e.g. Austin & Buscombe, 2008).

On natural beaches, the prevailing sorting mechanisms in the swash zone depend on various variables such as the beach morphology, the breaker type, and the grain-size distribution and nature of the sediment (Hughes *et al.*, 2000). It is commonly accepted that grain-size decreases landward on the beach profile as the result of decreasing intensity of the swash flow (Osborne & Simpson, 2005; Prodger *et al.*, 2017). However, divergence from this model is reported in the case of mixed grain-size settings. Guest & Hay (2021) investigated the small-scale morphodynamics of the swash zone of a mixed sand and gravel beach. Observations revealed a divergence of cobbles from the mid-swash towards the seaward and shoreward edges of the swash zone, and the subsequent fining of the mid-swash zone. This process highlights the influence of the substrate on the transport of coarse particles in a mixed grain-size setting. Coarse particle transport is favoured over fine substrate, where low angle of pivot and greater exposure to lift and drag forces causes the coarse particles to overpass the finer ones (Guest & Hay, 2021). In the context of mixed bioclastic–siliciclastic sediment, this sorting process is thought to be exacerbated by the low settling velocity and large drag coefficient of bioclastic particles (Rieux *et al.*, 2019).

Concerning lateral grading in overwash sediment, field observations in sandy environments show a decreasing grain size from the apex to the margins of sedimentation in the direction of transport, in relation with the decreasing intensity of washover flow (e.g. Leatherman & Williams, 1977). Proximal washover channels are generally characterized by lag concentration of shells and/or heavy minerals (e.g. Morton, 1978). Siliciclastic sands in washover generally show a small range of grain size, because of the well-sorted nature of aeolian sands that contribute to top deposits of the breached barrier (Sedgwick & Davis, 2003; Aagaard & Kroon, 2019). The coarsening trend towards the distal part of washover fans reported in the present study seems to be characteristic of the mixed bioclastic–siliciclastic sediment, with sorting processes similar to the ones described in the swash zone.

Sediment composition control on ridge morphology and structures

Several differences between ridge morphology and internal structures were observed between the three compositional mixtures. The bioclastic ridge is thick, with steep beach-face and landward slopes. Siliciclastic-dominated ridges are wider (Fig. 12). Washover beds become thinner and longer with increasing siliciclastic material, suggesting larger washover flow incursion. Similarly, the beach-face length increases with siliciclastic content, as a consequence of larger swash flow incursion. The volume of falling-stage deposits associated with the seaward migration of the ridge toe (Stage 4, Fig. 12) increases with increasing siliciclastic material. Bioclastic-dominated ridges keep up with the increasing water level, by simultaneous aggradation of washover sheets. With similar rates of water level elevation and increasing siliciclastic content, the ridges experience an intense roll-over (landward migration), and the ridge aggradation occurs mostly during the high water level stage.

The relationship between beach-face slope and sediment size has been the subject of

numerous studies (see Bujan *et al.*, 2019; McFall, 2019, for a review), and it has been widely demonstrated that coarser sediment sizes are associated with steeper beach-face slopes. On coarse-grained beaches, the high sediment permeability promotes swash infiltration and onshore transport, building a steep berm (Duncan, 1964; Quick, 1991; Turner & Masselink, 1998; Butt *et al.*, 2001; Masselink & Li, 2001). The empirical equations that predict the beach-face slope (see Bujan *et al.*, 2019, and references therein) most often imply a median grain-size diameter (d_{50}) and an estimation of the wave energy (through a significant wave height, a breaker height or a wave length). Some authors replaced the median grain diameter by the sediment fall velocity, and incorporated the effect of tidal range (Masselink & Short, 1993). The reduction of the sediment grain-size distribution to a median diameter is a reasonable assumption for siliciclastic sand in beach face environment, where the wave energy promotes an efficient sorting. However, it has serious limitation in the case of mixed beaches, and in mixed siliciclastic–bioclastic environments in particular, where grain size and sorting, as well as grain shape and packing, are key parameters affecting sediment porosity and permeability (Koltermann & Gorelick, 1995; Kamann *et al.*, 2007). In the case of a coarse packing (where the percentage of fine sediment is less than the porosity of the coarse sediment taken alone), the porosity decreases with increasing content of fine-sediment. On the contrary, in the case of a fine packing (where coarse particles are not self-supported), the porosity increases with decreasing content of coarse material. In mixed siliciclastic–bioclastic environments, the grain size of bioclastic particles, which have low settling velocity values, may be significantly coarser than the siliciclastic component considering the wave energy. Moreover, the size of bioclastic particles not only reflects the energy of the depositional environment, but is also dependent on the *in-situ* carbonate factory (e.g. De Falco *et al.*, 2011).

In the reported experiments, the morphology of the ridges associated with the three compositional mixtures suggests that sediment porosity and permeability decrease with increasing siliciclastic content. This is confirmed by the porosity values measured on the bulk compositional mixtures [$B_{25}S_{75}$ = 29% (±2); $B_{50}S_{50}$ = 33% (±2) and B_{100} = 44% (±2), respectively]. Moreover, large variations of permeability within the sedimentary bodies are expected, in relation with grain-size variations between and within the differential architectural elements (Weill *et al.*, 2012; Fick *et al.*, 2021). Consequently, the shorter and steeper beach-face of B_{100} is the consequence of an important infiltration of the swash flow, promoting a faster deposition of sediment. On the contrary, in the lower-permeability $B_{25}S_{75}$ sediment, a lower swash infiltration increases the run-up length and the backwash volume, and subsequently the beach-face width. The beach-face slope values are lower. Similarly, the same processes operate on the landward washover face. Overwash flows are strongly attenuated by infiltration into the B_{100} beach ridge (see Matias *et al.*, 2014), reducing the overwash incursion length, and enhancing vertical accretion of washover sheets, leading finally to a thicker beach ridge. On $B_{50}S_{50}$ and $B_{25}S_{75}$ beach ridges, due to a lower degree of infiltration, overwash flows have longer incursion lengths, leading to more elongated washover fans compared to B_{100}. Erosive channels may develop close to the barrier crest. Aggradation on the subaerial part of the washover deposits is reduced, resulting in thin and stretched washover sheets. The mixed sediment beach ridges are thus wider and lower-crested than fully bioclastic beach ridges. To the second order, infiltration processes may be influenced by local sediment properties, swell characteristics, or the degree of water saturation of the barrier, related for example to tidal water level fluctuations in the back-barrier (Masselink & Turner, 2012), processes which have not been investigated in this study.

Overall, the differences in sediment permeability and hydrodynamic behaviour of individual grains, which control sediment segregation, transport and depositional processes, explain the differences between the three compositional mixings of beach ridge dynamics and resulting internal architecture (Fig. 13).

CONCLUSION

The construction and resulting internal architectures of mixed siliciclastic–bioclastic coastal barriers were investigated in a wave flume. The influence of sediment composition was examined using three compositional mixtures with different proportions of bioclastic and siliciclastic sediment. The three experiments were subjected to similar cycles of water level rising and

falling under constant wave forcing, to trigger the construction of transgressive and regressive depositional units. The results obtained in this study are summarized as follows:

1 The three ridges obtained with different compositional mixings have developed similar first-order internal structures in response to mean water level fluctuations with an alternation of transgressive and regressive depositional units.

2 Owing to a larger porosity, bioclastic-rich mixtures promote larger infiltration of swash and washover flows. This results in a shorter and steeper beachface, and shorter and thicker washover deposits. Conversely, siliciclastic-dominated mixtures form thinner and more stretched morphologies, in relation with larger swash and washover flow incursions.

3 The largest flow infiltration in bioclastic-rich mixtures promotes faster sediment deposition. Consequently, bioclastic-rich barriers adapted faster to a disruption in their equilibrium morphology. The fast aggradation of washover sheets make bioclastic-rich ridges more resilient to submersion events than siliciclastic-dominated ridges.

4 Coarse-grained, thin and platy bioclastic particles are transported in the most distal parts of the swash zone and washover fans. Finer siliciclastic sand tends to accumulate in high-energy zones, such as the intermediate beachface and the channelized upper washover fans. The observed segregation patterns are both controlled by the grain size (the bioclastic fraction being coarser) and the composition (bioclastic grains being flat-shaped) of the mixed sediment.

These experiments suggest that the dynamics of a coastal barrier can be modified by a change in the balance between the siliciclastic and the carbonate sediment sources. This finding is particularly relevant for modern coastline, where anthropogenic impacts may reduce the terrigenous inputs and modify the carbonate factory through aquaculture, invasive species introduction, or modification of marine habitats and coastal water quality.

ACKNOWLEDGEMENTS

This study is a part of Alissia Rieux's PhD thesis funded by the Normandy Regional Council and the Ministry for the Ecological and Inclusive Transition (DDTM 35), in the framework of the research project "Sédibaie". The authors thank Laurent Perez (M2C) for the development of the topographic profiler acquisition software and GUI (SUMO), and Magalie Legrain (M2C) for the grain size analysis. We are grateful to the Chief Editor, Jaco Baas, the Associate Editor, Rick Sarg and to the journal reviewers for their helpful comments which improved an early version of the manuscript.

DATA AVAILABILITY STATEMENT

The data that supports the findings of this study are available in Figs S1–S9 of this article.

REFERENCES

Aagaard, T. and **Kroon, A.** (2019) Decadal behaviour of a washover fan, Skallingen Denmark. *Earth Surf. Process. Landf.*, **44**, 1755–1768.

Austin, M.J. and **Buscombe, D.** (2008) Morphological change and sediment dynamics of the beach step on a macrotidal gravel beach. *Mar. Geol.*, **249**, 167–183.

Baldock, T.E., **Birrien, F.**, **Atkinson, A.**, **Shimamoto, T.**, **Wu, S.**, **Callaghan, D.P.** and **Nielsen, P.** (2017) Morphological hysteresis in the evolution of beach profiles under sequences of wave climates - part 1; observations. *Coast. Eng.*, **128**, 92–105.

Bastos, A.C., **Quaresma, V.S.**, **Marangoni, M.B.**, **D'Agostini, D.P.**, **Bourguignon, S.N.**, **Cetto, P.H.**, **Silva, A.E.**, **Amado Filho, G.M.**, **Moura, R.L.** and **Collins, M.** (2015) Shelf morphology as an indicator of sedimentary regimes: a synthesis from a mixed siliciclastic–carbonate shelf on the eastern Brazilian margin. *J. South Am. Earth Sci.*, **63**, 125–136.

Berton, F., **Guedes, C.C.F.**, **Vesely, F.F.**, **Souza, M.C.**, **Angulo, R.J.**, **Rosa, M.L.C.C.** and **Barboza, E.G.** (2019) Quaternary coastal plains as reservoir analogs: wave-dominated sand-body heterogeneity from outcrop and ground-penetrating radar, Central Santos Basin, Southeast Brazil. *Sed. Geol.*, **379**, 97–113.

Billy, J., **Robin, N.**, **Hein, C.J.**, **Certain, R.** and **FitzGerald, D.M.** (2015) Insight into the late Holocene Sea-level changes in the NW Atlantic from a paraglacial beach-ridge plain south of Newfoundland. *Geomorphology*, **248**, 134–146.

Bonnot-Courtois, C., **Fournier, J.** and **Dréau, A.** (2004) Recent morphodynamics of shell banks in the western part of the bay of Mont-saint-Michel (France). *Geomorphol. Relief, Process. Environ*, **10**, 65–79.

Braithwaite, C.J.R. (1973) Settling behaviour related to sieve analysis of skeletal sands. *Sedimentology*, **20**, 251–262.

Bristow, C.S., **Chroston, P.N.** and **Bailey, S.D.** (2000) The structure and development of foredunes on a locally prograding coast: insights from ground-penetrating radar surveys, Norfolk, UK. *Sedimentology*, **47**, 923–944.

Bujan, N., **Cox, R.** and **Masselink, G.** (2019) From fine sand to boulders: examining the relationship between beach-face slope and sediment size. *Mar. Geol.*, **417**, 106012.

Butt, T., **Russell, P.** and **Turner, I.** (2001) The influence of swash infiltration–exfiltration on beach face sediment transport: onshore or offshore? *Coast. Eng.*, **42**, 35–52.

Carranza-Edwards, A. (2001) Grain size and sorting in modern beach sands. *J. Coast. Res.*, **17**, 38–52.

Carter, R.W.G. (1986) The morphodynamics of beach-ridge formation: Magilligan, Northern Ireland. *Mar. Geol.*, **73**, 191–214.

Chiarella, D. and **Longhitano, S.G.** (2012) Distinguishing depositional environments In shallow-water mixed, bio-siliciclastic deposits on the basis of the degree of Heterolithic segregation (Gelasian, southern Italy). *J. Sed. Res.*, **82**, 969–990.

Chiarella, D., **Longhitano, S.G.** and **Tropeano, M.** (2017) Types of mixing and heterogeneities in siliciclastic-carbonate sediments. *Mar. Pet. Geol.*, **88**, 617–627.

Cooper, N.J. (2005) Wave dissipation across intertidal surfaces in the wash tidal inlet, eastern England. *J. Coast. Res.*, **21**, 28–40.

Cooper, J.A.G., **Green, A.N.** and **Loureiro, C.** (2018) Geological constraints on mesoscale coastal barrier behaviour. *Glob. Planet. Change*, **168**, 15–34.

Costas, S., **Ferreira, Ó.**, **Plomaritis, T.A.** and **Leorri, E.** (2016) Coastal barrier stratigraphy for Holocene high-resolution sea-level reconstruction. *Sci. Rep.*, **6**, 38726.

De Falco, G., **De Muro, S.**, **Batzella, T.** and **Cucco, A.** (2011) Carbonate sedimentation and hydrodynamic pattern on a modern temperate shelf: the strait of Bonifacio (western Mediterranean). *Estuar. Coast. Shelf Sci.*, **93**, 14–26.

De Falco, G., **Molinaroli, E.**, **Conforti, A.**, **Simeone, S.** and **Tonielli, R.** (2017) Biogenic sediments from coastal ecosystems to beach–dune systems: implications for the adaptation of mixed and carbonate beaches to future sea level rise. *Biogeosciences*, **14**, 3191–3205.

Dougherty, A.J. (2014) Extracting a record of Holocene storm erosion and deposition preserved in the morphostratigraphy of a prograded coastal barrier. *Cont. Shelf Res.*, **86**, 116–131.

Duncan, J.R. (1964) The effects of water table and tide cycle on swash-backwash sediment distribution and beach profile development. *Mar. Geol.*, **2**, 186–197.

Fick, C., **Puhl, E.** and **Toldo, E.E.** (2020) Threshold of motion of bivalve and gastropod shells under oscillatory flow in flume experiments. *Sedimentology*, **67**, 627–648.

Fick, C., **Puhl, E.**, **Toldo-Junior, E.E.**, **Pereira, L.M.**, **Oliveira, V.C.B.** and **Cruz, F.E.G.** (2021) Study of shelly shore ridge formation using wave flume experiments: morphological evolution and depositional patterns. *Geomorphology*, **392**, 107926.

Flemming, B.W. (2017) Particle shape-controlled sorting and transport behaviour of mixed siliciclastic/bioclastic sediments in a mesotidal lagoon, South Africa. *Geo-Mar. Lett.*, **37**, 397–410.

Fruergaard, M., **Tessier, B.**, **Poirier, C.**, **Mouazé, D.**, **Weill, P.** and **Noël, S.** (2020) Depositional controls on a hypertidal barrier-spit system architecture and evolution, pointe du banc spit, North-Western France. *Sedimentology*, **67**, 502–533.

Goslin, J. and **Clemmensen, L.B.** (2017) Proxy records of Holocene storm events in coastal barrier systems: storm-wave induced markers. *Quat. Sci. Rev.*, **174**, 80–119.

Grasso, F., **Michallet, H.** and **Barthélemy, E.** (2011) Experimental simulation of shoreface nourishments under storm events: a morphological, hydrodynamic, and sediment grain size analysis. *Coast. Eng.*, **58**, 184–193.

Guest, T.B. and **Hay, A.E.** (2021) Small-scale Morpho-sedimentary dynamics in the swash zone of a Megatidal mixed sand–Gravel Beach. *J. Mar. Sci. Eng.*, **9**, 413.

Hede, M.U., **Bendixen, M.**, **Clemmensen, L.B.**, **Kroon, A.** and **Nielsen, L.** (2013) Joint interpretation of beach-ridge architecture and coastal topography show the validity of sea-level markers observed in ground-penetrating radar data. *Holocene*, **23**, 1238–1246.

Hine, A.C. (1979) Mechanisms of berm development and resulting beach growth along a barrier spit complex. *Sedimentology*, **26**, 333–351.

Houser, C. and **Hill, P.** (2010) Wave attenuation across an intertidal sand flat: implications for mudflat development. *J. Coast. Res.*, **263**, 403–411.

Hughes, S.A. (1993) Physical models and laboratory techniques in coastal engineering. In: *Advanced Series on Ocean Engineering*, p. 568. World Scientific, Singapore.

Hughes, M.G., **Keene, J.B.** and **Joseph, R.G.** (2000) Hydraulic sorting of heavy-mineral grains by swash on a medium-Sand Beach. *J. Sed. Res.*, **70**, 994–1004.

Jahnert, R., **de Paula, O.**, **Collins, L.**, **Strobach, E.** and **Pevzner, R.** (2012) Evolution of a coquina barrier in Shark Bay, Australia by GPR imaging: architecture of a Holocene reservoir analog. *Sed. Geol.*, **281**, 59–74.

Jol, H.M., **Smith, D.G.** and **Meyers Richard, A.** (1996) Digital ground penetrating radar (GPR): a new geophysical tool for coastal barrier research (examples from the Atlantic, gulf and Pacific coasts, U.S.A.). *J. Coast. Res.*, **12**, 960–968.

Joshi, S., **Duffy, G.P.** and **Brown, C.** (2017) Critical bed shear stress and threshold of motion of maerl biogenic gravel. *Estuar. Coast. Shelf Sci.*, **194**, 128–142.

Kamann, P.J., **Ritzi, R.W.**, **Dominic, D.F.** and **Conrad, C.M.** (2007) Porosity and permeability in sediment mixtures. *Ground Water*, **45**, 429–438.

Kench, P. and **McLean, R.** (1996) Hydraulic characteristics of bioclastic deposits: new possibilities for environmental interpretation using settling velocity fractions. *Sedimentology*, **43**, 561–570.

Kirby, R. (2000) Practical implications of tidal flat shape. *Cont. Shelf Res.*, **20**, 1061–1077.

Kleinhans, M.G., **van Dijk, W.M.**, **van de Lageweg, W.I.**, **Hoyal, D.C.J.D.**, **Markies, H.**, **van Maarseveen, M.**, **Roosendaal, C.**, **van Weesep, W.**, **van Breemen, D.**, **Hoendervoogt, R.** and **Cheshier, N.** (2014) Quantifiable effectiveness of experimental scaling of river- and delta morphodynamics and stratigraphy. *Earth Sci. Rev.*, **133**, 43–61.

Kleinhans, M.G., **van Scheltinga, R.T.**, **van der Vegt, M.** and **Markies, H.** (2015) Turning the tide: growth and dynamics of a tidal basin and inlet in experiments. *Case Rep. Med.*, **120**, 95–119.

Koltermann, C.E. and **Gorelick, S.M.** (1995) Fractional packing model for hydraulic conductivity derived from sediment mixtures. *Water Resour. Res.*, **31**, 3283–3297.

Komar, P.D. (1989) Physical processes of waves and currents and the formation of marine placers. *Rev. Aquat. Sci.*, **1**, 393–423.

de Kruijf, M., **Slootman, A.**, **de Boer, R.A.** and **Reijmer, J.J.G.** (2021) On the settling of marine carbonate grains: review and challenges. *Earth Sci. Rev.*, **217**, 103532.

Larsonneur, C., **Bouysse, P.** and **Auffret, J.-P.** (1982) The superficial sediments of the English Channel and its Western approaches. *Sedimentology*, **29**, 851–864.

Leatherman, S.P. and **Williams, A.T.** (1977) Lateral textural grading in overwash sediments. *Earth Surf. Process.*, **2**, 333–341.

Li, Y., **Yu, Q.**, **Gao, S.** and **Flemming, B.W.** (2020) Settling velocity and drag coefficient of platy shell fragments. *Sedimentology*, **67**, 2095–2110.

Lindhorst, S., **Betzler, C.** and **Hass, H.C.** (2008) The sedimentary architecture of a Holocene barrier spit (Sylt, German bight): swash-bar accretion and storm erosion. *Sed. Geol.*, **206**, 1–16.

Longhitano, S.G. (2011) The record of tidal cycles in mixed silici-bioclastic deposits: examples from small Plio-Pleistocene peripheral basins of the microtidal Central Mediterranean Sea: tidal cycles in mixed silici-bioclastic deposits. *Sedimentology*, **58**, 691–719.

Maiklem, W.R. (1968) Some hydraulic properties of bioclastic carbonate grains. *Sedimentology*, **10**, 101–109.

Masselink, G. and **Li, L.** (2001) The role of swash infiltration in determining the beachface gradient: a numerical study. *Mar. Geol.*, **176**, 139–156.

Masselink, G. and **Short, A.D.** (1993) The effect of tide range on beach morphodynamics and morphology: a conceptual beach model. *J. Coast. Res.*, **9**, 785–800.

Masselink, G. and **Turner, I.L.** (2012) Large-scale laboratory investigation into the effect of varying back-barrier lagoon water levels on gravel beach morphology and swash zone sediment transport. *Coast. Eng.*, **63**, 23–38.

Masselink, G., **Kroon, A.** and **Davidson-Arnott, R.G.D.** (2006) Morphodynamics of intertidal bars in wave-dominated coastal settings — a review. *Geomorphology*, **73**, 33–49.

Masselink, G., **Ruju, A.**, **Conley, D.**, **Turner, I.**, **Ruessink, G.**, **Matias, A.**, **Thompson, C.**, **Castelle, B.**, **Puleo, J.**, **Citerone, V.** and **Wolters, G.** (2016) Large-scale barrier dynamics experiment II (BARDEX II): experimental design, instrumentation, test program, and data set. *Coast. Eng.*, **113**, 3–18.

Matias, A., **Blenkinsopp, C.E.** and **Masselink, G.** (2014) Detailed investigation of overwash on a gravel barrier. *Mar. Geol.*, **350**, 27–38.

Matias, A., **Masselink, G.**, **Castelle, B.**, **Blenkinsopp, C.E.** and **Kroon, A.** (2016) Measurements of morphodynamic and hydrodynamic overwash processes in a large-scale wave flume. *Coast. Eng.*, **113**, 33–46.

McFall, B.C. (2019) The relationship between beach grain size and intertidal beach face slope. *J. Coast. Res.*, **35**, 1080–1086.

McKee, E.D. and **Sterrett, T.** (1961) Laboratory experiments on form and structure of longshore bars and beaches. In: *Geometry of Sandstone Bodies* (Eds Peterson, J.A. and Osmond, J.C.), *AAPG SP*, **22**, 13–28.

Morton, R.A. (1978) Large-scale rhomboid bed forms and sedimentary structures associated with hurricane washover. *Sedimentology*, **25**, 183–204.

Morton, R.A., **Gonzalez, J.L.**, **Lopez, G.I.** and **Correa, I.D.** (2000) Frequent non-storm washover of barrier islands, Pacific coast of Colombia. *J. Coast. Res.*, **16**, 82–87.

Mury, A., **Jeanson, M.**, **Collin, A.**, **James, D.** and **Etienne, S.** (2019) High resolution shoreline and Shelly ridge monitoring over stormy winter events: a case study in the Megatidal Bay of Mont-saint-Michel (France). *J. Mar. Sci. Eng.*, **7**, 97.

do Nascimento Silva, L.L. and **Gomes, M.P.** (2020) Statistical approach on mixed carbonate-siliciclastic sediments of the NE Brazilian outer shelf. *Geo-Mar. Lett.*, **40**, 1001–1013.

Neal, A. (2004) Ground-penetrating radar and its use in sedimentology: principles, problems and progress. *Earth Sci. Rev.*, **66**, 261–330.

Neal, A., **Richards, J.** and **Pye, K.** (2002) Structure and development of shell cheniers in Essex, Southeast England, investigated using high-frequency ground-penetrating radar. *Mar. Geol.*, **185**, 435–469.

Oliver, T.S.N., **Kennedy, D.M.**, **Tamura, T.**, **Murray-Wallace, C.V.**, **Konlechner, T.M.**, **Augustinus, P.C.** and **Woodroffe, C.D.** (2018) Interglacial-glacial climatic signatures preserved in a regressive coastal barrier, southeastern Australia. *Palaeogeogr. Palaeoclimatol. Palaeoecol.*, **501**, 124–135.

Osborne, P.D. and **Simpson, D.P.** (2005) Cross-shore variation of grain size on beaches. In: *Encyclopedia of Coastal Science* (Ed. Schwartz, M.L.), pp. 353–354. Springer, Dordrecht.

Paola, C., **Straub, K.**, **Mohrig, D.** and **Reinhardt, L.** (2009) The "unreasonable effectiveness" of stratigraphic and geomorphic experiments. *Earth Sci. Rev.*, **97**, 1–43.

Paphitis, D., **Collins, M.B.**, **Nash, L.A.** and **Wallbridge, S.** (2002) Settling velocities and entrainment thresholds of biogenic sands (shell fragments) under unidirectional flow: settling velocities and entrainment threshold of biogenic sands. *Sedimentology*, **49**, 211–225.

Pedley, M. and **Carannante, G.** (2006) Cool-water carbonate ramps: a review. In: *Cool-Water Carbonates: Depositional Systems and Palaeoenvironmental Controls* (Eds Pedley, H.M. and Carannante, G.), pp. 1–9. Geology Society of Special Publications, London.

Pilkey, O.H., **Morton, R.W.** and **Luternauer, J.** (1967) The carbonate fraction of beach and dune sands. *Sedimentology*, **8**, 311–327.

Prodger, S., **Russell, P.** and **Davidson, M.** (2017) Grain-size distributions on high-energy sandy beaches and their relation to wave dissipation. *Sedimentology*, **64**, 1289–1302.

Quick, M.C. (1991) Onshore-offshore sediment transport on beaches. *Coast. Eng.*, **15**, 313–332.

Rieux, A., **Weill, P.**, **Mouaze, D.**, **Poirier, C.**, **Nechenache, F.**, **Perez, L.** and **Tessier, B.** (2019) Threshold of motion and settling velocities of mollusc shell debris: influence of faunal composition. *Sedimentology*, **66**, 895–916.

Rivers, J., **Engel, M.**, **Dalrymple, R.**, **Yousif, R.**, **Strohmenger, C.J.** and **Al-Shaikh, I.** (2020) Are carbonate barrier islands mobile? Insights from a mid to late-Holocene system, Al Ruwais, northern Qatar. *Sedimentology*, **67**, 534–558.

Schwartz, R.K. (1982) Bedform and stratification characteristics of some modern small-scale washover sand bodies. *Sedimentology*, **29**, 835–849.

Sedgwick, P.E. and **Davis, R.A.** (2003) Stratigraphy of washover deposits in Florida: implications for recognition in the stratigraphic record. *Mar. Geol.*, **200**, 31–48.

Short, A.D. (2002) The distribution and impact of carbonate sands on southern Australian beach-dune systems. In: *Carbonate Beaches 2000* (Eds Magoon, O.T., Robbins, L.L. and Ewing, L.), pp. 236–250. ASCE, Reston.

Slingerland, R. and **Smith, N.D.** (1986) Occurrence and formation of water-laid placers. *Annu. Rev. Earth Planet. Sci.*, **14**, 113–147.

Smith, D.A. and **Cheung, K.F.** (2004) Initiation of motion of calcareous sand. *J. Hydraul. Eng.*, **130**, 467–472.

Stutz, M.L. and **Pilkey, O.H.** (2001) A review of global barrier Island distribution. *J. Coast. Res., S.I.*, **34**, 15–22.

Tamura, T. (2012) Beach ridges and prograded beach deposits as palaeoenvironment records. *Earth Sci. Rev.*, **114**, 279–297.

Tessier, B., **Poirier, C.**, **Weill, P.**, **Dezileau, L.**, **Rieux, A.**, **Mouazé, D.**, **Fournier, J.** and **Bonnot-Courtois, C.** (2019) Evolution of a Shelly Beach ridge system over the last decades in a Hypertidal open-coast embayment (Western Mont-saint-Michel Bay, NW France). *J. Coast. Res.*, **88**, 77.

Turner, I.L. and **Masselink, G.** (1998) Swash infiltration-exfiltration and sediment transport. *J. Geophys. Res.*, **103**, 30813–30824.
VanDusen, B.M., **Theuerkauf, E.J.**, **Fegley, S.R.** and **Rodriguez, A.B.** (2016) Monitoring overwash using water-level loggers resolves frequent inundation and run-up events. *Geomorphology*, **254**, 32–40.
Wang, J., **You, Z.-J.** and **Liang, B.** (2020) Laboratory investigation of coastal beach erosion processes under storm waves of slowly varying height. *Mar. Geol.*, **430**, 106321.
Weill, P., **Mouazé, D.**, **Tessier, B.** and **Brun-Cottan, J.-C.** (2010) Hydrodynamic behaviour of coarse bioclastic sand from shelly cheniers. *Earth Surf. Process. Landforms*, **35**, 1642–1654.
Weill, P., **Tessier, B.**, **Mouazé, D.**, **Bonnot-Courtois, C.** and **Norgeot, C.** (2012) Shelly cheniers on a modern macrotidal flat (Mont-saint-Michel bay, France) — internal architecture revealed by ground-penetrating radar. *Sed. Geol.*, **279**, 173–186.
Weill, P., **Mouazé, D.** and **Tessier, B.** (2013) Internal architecture and evolution of bioclastic beach ridges in a megatidal chenier plain: field data and wave flume experiment. *Sedimentology*, **60**, 1213–1230.
Williams, J.J., **Buscombe, D.**, **Masselink, G.**, **Turner, I.L.** and **Swinkels, C.** (2012) Barrier dynamics experiment (BARDEX): aims, design and procedures. *Coast. Eng.*, **63**, 3–12.

Manuscript received 13 July 2022; revision accepted 25 January 2023

Supporting Information

Additional information may be found in the online version of this article:

Fig. S1. Lacquer peel of the B_{100} barrier at the end of Stage 11 and interpretation of the internal architecture. Stages 8 to 11 correspond to an additional cycle of water level not discussed in the paper.

Fig. S2. Lacquer peel of the $B_{50}S_{50}$ barrier at the end of Stage 7 and interpretation of the internal architecture.

Fig. S3. Lacquer peel of the $B_{25}S_{75}$ barrier at the end of Stage 7 and interpretation of the internal architecture.

Fig. S4. Uninterpreted side photographs of the B_{100}, $B_{50}S_{50}$ and $B_{25}S_{75}$ barriers at the end of Stage 1.

Fig. S5. Uninterpreted side photographs of the B_{100}, $B_{50}S_{50}$ and $B_{25}S_{75}$ barriers at the end of Stage 3.

Fig. S6. Uninterpreted side photographs of the B_{100}, $B_{50}S_{50}$ and $B_{25}S_{75}$ barriers at the end of Stage 5.

Fig. S7. Uninterpreted side photographs of the B_{100}, $B_{50}S_{50}$ and $B_{25}S_{75}$ barriers at the end of Stage 7.

Fig. S8. Grain-size distribution along the final B_{100} barrier surface.

Fig. S9. Grain-size distribution along the final $B_{25}S_{75}$ barrier surface.